Using HHT to Successfully Uncouple Seasonal and Interannual Components in Remotely Sensed Data

Jorge E. Pinzón
NASA-GSFC Code 923, SSAI
Greenbelt, MD 20771, USA

ABSTRACT

This paper shows how the EMD can successfully uncouple the seasonal and interannual components of NDVI signals from induced satellite artifacts. The known delay in crossing the equator of the afternoon National Oceanic and Atmospheric Administration (NOAA) polar satellites results in changes of illumination that affects measurements made by the advanced very high resolution radiometer (AVHRR). Despite the improved processing, correction of calibration loss and atmospheric effects, one of the standard AVHRR products, the normalized difference vegetation index (NDVI) time series, still may contain variations due to orbital drift or changes in sun-target-sensor geometry. In this study, we identify solar zenith angle (SZA) trends associated to orbital drifts and analize their effects on NDVI. We present the adaptive empirical mode decomposition (EMD) method as a mean to identify and remove the induced SZA trend from NDVI time series. The EMD is based on the local characteristic time scale of the data, and it is usable to give sharp identifications of embedded structures of nonlinear and nonstationary processes. The approach was tested on 1 degree NDVI global data sets. The results show : (1) that regions in the tropics, especially tropical forest, are the most SZA-affected, and (2) the high northern latitudes are less contaminated.

Keywords: Normalized difference vegetation index; seasonal patterns; solar zenith angle;orbital drift; empirical mode decomposition

1. INTRODUCTION

The capability of satellite observations to monitor the dynamics of the Earth's surface provides a basis for understanding temporal trends in vegetation and their significance. In the 20 year time series of NDVI from NOAA-AVHRR data is critically important that these measurements represent accurately the Earth's environment at the time of imaging. The high temporal frequency has made AVHRR data invaluable in the study of large area vegetation dynamics [1], [2]. This satellite-sensor system was primarily designed for cloud, atmospheric and sea-surface temperature analysis; however, the PM platforms of the NOAA satellites have provided the spatial coverage and spectral resolution needed for monitoring global vegetation dynamics on a daily basis. Vegetation indices are by far the most widely-used product of the AVHRR sensor [3]. Most of these applications are based on the normalized difference vegetation index (NDVI), which is the ratio of the near infrared (NIR) and visible (VIS) radiances, $NDVI = \frac{NIR - VIS}{NIR + VIS}$. This ratio yields a measure of photosynthetic capacity such that the higher the value of the ratio, the more photosynthetically active the cover type [4].

Still, high data frequency have not come without drawbacks. Known limitations of the AVHRR instrument due to the orbital drift in the PM platforms, the coarse resolution, and wide bandwidths in the VIS and NIR wavelengths generate significant inaccuracies in NDVI interpretation: (1) a greater probability of sub-pixel clouds that interfere with the vegetation signal, (2) significant variation in the sun-target-view geometries and illumination of AVHRR measurements combined with surface bidirectional reflectance (BRDF) properties of the land surface, topography, and soil background reflectance [5]. In order to reduce these inaccuracies, atmospheric correction and standard compositing techniques are common practice in all NDVI processing systems [6], [7]. Among them, the maximum NDVI compositing (MVC) technique has been used in nearly all operational AVHRR processing chains [2]. The MVC procedure requires the processing of a series of multitemporal georeferenced satellite data into NDVI images. On a pixel-by-pixel basis, each NDVI value is examined, and only the highest value is retained for each pixel location. Holben [8] showed that MVC imagery is highly related to green vegetation dynamics, and the aforementioned problems have been minimized. Moreover, Pinzón et al. [9] showed that MVC provides the image with highest spatial coherence among the compositing techniques most commonly used.

Despite the improved processing, correction of calibration loss and atmospheric effects, NDVI still may contain variations due to orbital drift and changes in sun-target-sensor geometry, since the closure of such a system involves more unknowns than measurable quantities [5], [10], [11]. Removing these nonvegetative effects from the time series remains a challenge, since an analytical or numerical solution to the system would be prohibitive in real time processing, given the huge amount of data to process, both spatially and temporally.

Alternatively, to eliminate the interferences due to orbital drift, one could ignore the underlying governing equations entirely and experimentally try to find an effective description of the interactions between the NDVI and SZA trends [12]. This paper proposes the adaptive EMD method as an

approach to identify and remove the SZA-drift components from the NDVI. To be precise, we decompose NDVI and SZA signals in terms of intrinsic mode functions (IMF) using the EMD to simplify and describe more accurately the NDVI-SZA relationship. In particular, we can tune the EMD to uncouple the seasonal and interannual components of NDVI signals from SZA-drift induced structures.

The primary objective of this study is to examine and correct the influence of changing SZA due to orbital drift on measured NDVI data. The standard processing of NDVI imagery is briefly described; the EMD technique is introduced with examples of trend detection in SZA latitudinal profiles as a means to measure and correct orbital drift impact; a correction approach is tested and evaluated within the framework of SZA-filtering on 1^o NDVI data sets.

2. EMPIRICAL MODE DECOMPOSITION

Due to the limitations of the available methods to analyze non-linear and non-stationary data, Huang et al. [13] proposed a new alternative for a faithful representation of data with these characteristics that besides shows clearly a physical scale or frequency content.

EMD decomposes a signal into local intrinsic mode functions (IMF) plus an intrinsic trend acting at different (instantaneous) frequencies. Different from other data analysis methods, this method is totally adaptive: it derives the IMF basis from the data itself. IMFs are computed from successive (sifting) differences of local means derived locally from upper and lower envelopes of the signal [13], [14]. The result is an IMF with (a) a number of extrema and a number of zero-crossings either equals or differing at most by one and (b) with zero local mean value defined from the envelopes of local maxima and local minima at any point. With these two properties, the derived IMFs will have a well behaved Hilbert (instantaneous) spectrum [13]. These properties allow us to identify and remove artifacts connected to the drift of NOAA satellites. The developed EMD filter extracts seasonal and interannual variations as byproducts of the NDVI signal. These features open new possibilities of analysis at different temporal scales.

3. PROCESSING OF NDVI IMAGERY

The data examined here are obtained from the Global Inventory Mapping and Monitoring Study (GIMMS) processing system using 15-day compositing at 1^o. The GIMMS processing system uses MVC as compositing technique and cloud screening prior to compositing, using an AVHRR channel 5 thermal threshold value over Africa (283K) and South America (273K). Pixels having scan angles greater than 45 degrees from nadir view and pixels associated with unrealistic reflectance values were also screened prior to compositing [15].

Figure 1 shows uncorrected NDVI data at various 1^o latitudes and longitudes. Vegetated tropical areas (Figure 1(b-f)), and especially tropical forests (Figure 1(c-f)) present an evident trend connected to the orbital drift or SZA variation. Desert areas (Figure 1(a)) and Northern latitudes (Figure 1(g-i)) appear less affected by changes in SZA. In fact, previous studies in growing season patterns

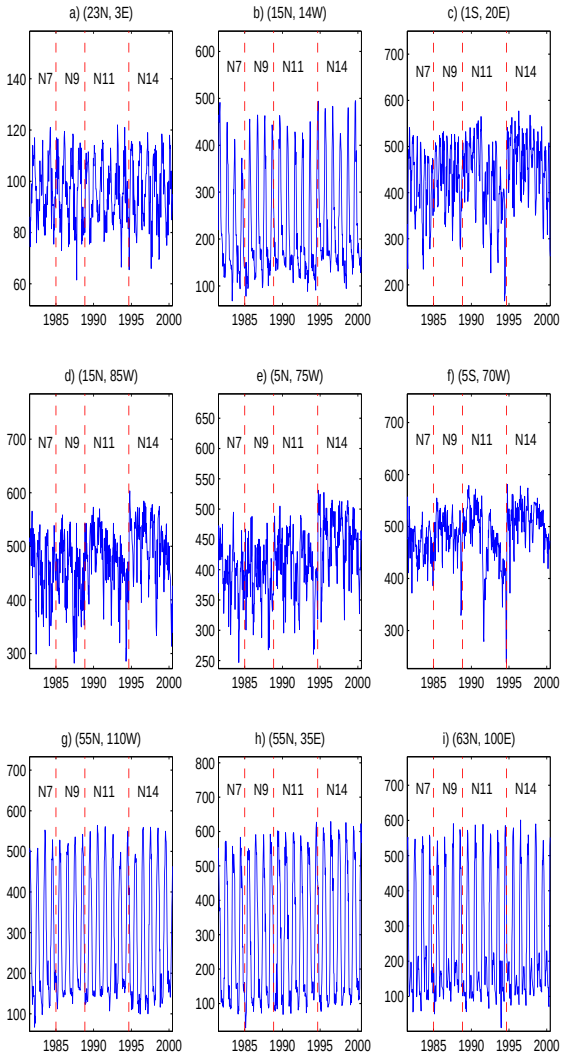

Fig. 1. Uncorrected NDVI data at particular 1^o latitudes and longitudes. Vegetated tropical areas (b-f), and especially tropical forests (c-f), present an evident trend connected to the SZA variation. Desert areas (a) and Northern latitudes (g-i) appear less affected by changes in SZA.

using NDVI from AVHRR [16], [17], [18], [19] indicate that there is no statistically meaningful relation between NDVI and SZA. In other words, since the magnitude of SZA trends at those higher latitudes is very small compared with the high seasonal variation in the NDVI of vegetated areas, its contribution is minimal to the NDVI signal at those latitudes (see Figure 2). However, explicit quantification of these contributions has not been reported. Moreover, Gutman [20], using other AVHRR data set, questioned the reliability of NDVI data for inferring the northern latitude greening trend since potential artifacts related to SZA and intersensor changes could remain in the data.

4. IMPACT OF ORBITAL DRIFT ON NDVI AND EMD-SZA FILTERING

As discussed here, the EMD method adjusts itself to local extrema and generates zero references and trends by the sifting process. Figure 2 shows the effects of the satellite drift on the SZA at different 10^o latitude bands. An increasing trend is observed in each satellite due to its delay in the equatorial crossing time. This trend, overimposed on each plot, is accurately extracted and associated as the EMD-trend. It is noteworthy to observe that drifts effects are more pronounced at lower latitudes (higher slopes), whereas seasonal variations dominate at higher latitudes. Note also that equatorial plots (10S to 10N) have an extra oscillation due to solar nadir moving past the target latitude, causing an increase in SZA at six month intervals rather than at yearly intervals [5]. The components of the EMD, as Figure 2 shows, are usually physically meaningful, since each scale is defined by the physical data itself.

Similarly, the EMD is used to extract NDVI trends that may be associated to satellite orbital drift, reducing the interference of these components in the NDVI signal. Then, the corrected NDVI time series is decomposed into two EMD-components: a wave-seasonal and trend. If the NDVI is affected by orbital drift, its trend component inherits solely this artifact. Following Huang et al. suggestion [13], the SZA artifact can be removed by using IMF as a time-space filter. In this case, NDVI trends and SZA trends are correlated and the corresponding SZA trend is filtered out from NDVI signals by EMD-filtering.

Table 1 shows the results of the SZA EMD-filtering approach for selected 1^o degree latitude-longitude pixels from regions representing different biomes. It is found that the percentage variance of NDVI variability explained by the filtered t_{szac} component decreases as latitude increases (l - p) and as vegetation biomes decreases (a, b). This implies that t_{szac} variability is very small at those northern latitude regions and the NDVI is minimally sensitive as vegetation biomes decreases. This result is confirmed by the coefficient of determination between t_{szac} and the correspondent 10^o latitude SZA trends. In most of those regions r^2 is less than 75. This is not the case for tropical areas (c - j), especially tropical forest (c - g), where the percentage variance explained is greater than 10 and the r^2 above 85.

Figure 3 shows in each panel, the uncorrected NDVI and its associated trend (U-time series), the solar zenith angle component t_{szac} removed (S in the figure) and the correspondent corrected NDVI and trend (C-time series). Each panel represents the same 1^o degree time series at the latitude-longitude pixels described in Table 1. This confirms the main conclusion of Table 1: regions in the tropics, especially tropical forest, are the most SZA-affected, (2) the high northern latitudes and regions with low vegetation biomes are less contaminated, and (3) all remaining components in the C-time series are found to be statistically independent of the SZA. Therefore, the EMD-filtering approach presented here constitutes a sound SZA correction technique, especially in tropical forests where the NDVI signal is shown to be more affected. It is worthy to notice

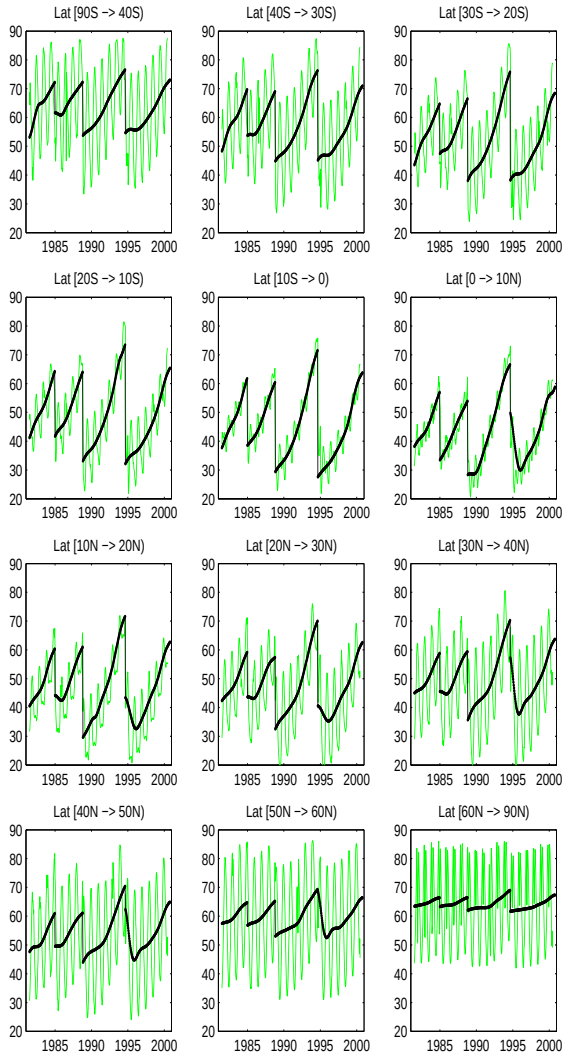

Fig. 2. Solar zenith angle drift by 10^o latitude bands. Drifts effects are more pronounced at lower latitudes (higher slopes), whereas seasonal variations dominate at higher latitudes. An extra oscillation is observed in equatorial plots (10S to 10N) due to solar nadir moving past the target latitude.

from Figure 3 that the SZA EMD-filtering keeps known salient features found with the NDVI time series like the drop in the Sahel in 1984-1985 (b) due to a serious drought [21], the north-eastern Brazil NDVI trends (h) related to the El Niño south oscillation (ENSO) [22], and the aforementioned long term stability of deserts (a), and tropical forests (c-g) [2]. There is much further work that needs to be done for a deeper analysis of the corrected C-time series, but that is beyond the scope of this work. From the corrected trends we can still see an expected discontinuity around September of 1994. This discontinuity is due to the lost of NOAA-11 and the lack of new satellites that could take its place and continue the recollection of data. The only option available to preserve the continuity of the time series was the old NOAA-9 passing now the equator in descending node. Late January of 1995, NOAA-14 was operational and took NOAA-9's place.

TABLE I

PERCENTAGE VARIANCE OF NDVI EXPLAINED BY THE FILTERED t_{szac} COMPONENT, COEFFICIENT OF DETERMINATION OF ORBITAL DRIFT SZA TRENDS AND EXTRACTED NDVI t_{szac}. ALL COEFFICIENTS ARE SIGNIFICANT WITH $p < 0.00001$.

		t_{szac}	
Location	(Lat, Lon)	%	r^2
a) Sahara	(23N, 3E)	2	72
b) Sahel	(15N, 14W)	3	84
c) Central Forest	(1S, 20E)	14	87
e) Center America	(15N, 85W)	18	86
g) Amazon	(5S, 70W)	23	87
i) Indochina	(15S, 105E)	9	74
j) Australia	(25S, 135E)	26	92
l) Great plains	(45N, 105W)	2	80
m) Canada	(55N, 110W)	1	68
o) Central Russia	(55N, 35E)	1	68
p) Siberia	(63N, 100E)	1	51

5. DISCUSSION AND CONCLUSIONS

In summary, Figure 4 shows in what percentage and what regions the SZA artifact affects the NDVI signal. The coefficient of determination between correspondent SZA trends at 10^o latitude bands and (a) uncorrected NDVI, (b) filtered out SZA component, and (c) corrected NDVI are shown. The tropics and especially tropical forests are the most affected. The corrected NDVI as expected shows a low correlation.

Figure 4(d) shows the variability of the NDVI signal given by the temporal standard deviation of each pixel. Deserts are the most stable as many studies have assumed. The Australian desert shows that a SZA correction is needed. The desert calibration used in GIMMS data stream is based on an expected stable region of the Sahara desert [15], which shows very different characteristics from the Australian desert. This confirms that one cannot assume that any spurious trend in NDVI over stable targets, e.g. deserts, can be linearly extrapolated and corrected in all surfaces, not even in similar surfaces as previous efforts have suggested. This figure also shows that tropical forests are not as stable. However, as the SZA artifacts are removed from the data, most of this variance is attenuated (see Figure 4e) and its stability increases (Figure 4f).

In Figure 4 (d,e,f), one can see a clear horizontal artifact on the South American continent around Colombia. Restricted subsetting of the raw AVHRR 1b orbits during the 1980s resulted in data gaps along the northern South American continent from 1981-1989. When computing resources became more abundant in the 1990s, Central America and northern South America were reprocessed to fill in the missing area. The horizontal bands seen in the 1-degree data are the residual data drops resulting from these two processing streams.

Concluding, we have presented an EMD approach to improve AVHRR-NDVI time series by removing spurious SZA trends induced by satellite drift. By using this decomposition, we found a mean trend in the NDVI that can be explained almost entirely by SZA trends. The remaining IMF components of the NDVI were found to be statistically independent of the SZA. Although the correction eliminates up to 30 percent of the variability in NDVI signals, it keeps all known vegetation features captured by the NDVI time series. Therefore, we have shown that the EMD-filtering approach of the associated mean SZA trend from NDVI time series constituted a sound SZA correction technique. In particular, we have removed SZA trends from tropical areas, especially forests, where the NDVI signal was shown to be more affected. As an additional gain, we have shown that the corrected NDVI and associated

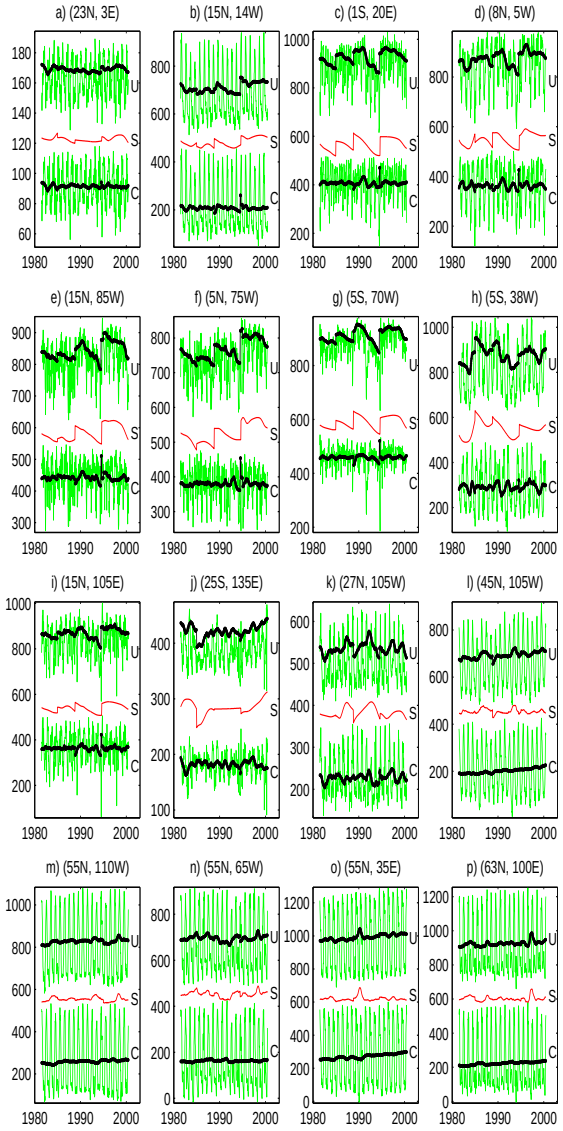

Fig. 3. Each panel shows the uncorrected NDVI and its associated trend (U-time series), filtered SZA component t_{szac} (S-time series) and SZA corrected NDVI and its associated corrected trend (C-time series) at different 3^o by 3^o latitude-longitude regions. U- and S-time series are shifted by the range of variation of the particular NDVI in each pannel.

IMFs features can be used in concert for better spatial characterization and time series analysis.

6. REFERENCES

[1] C. J. Tucker, "History of the use of AVHRR data for land applications," in *Advances in the use of NOAA AVHRR data for land applications* (G. D'Souza, A. S. Belward, and J.-P. Malingreau, eds.), pp. 1–19, ECSC, EEC, EAEC, Brussels, 1996.

[2] S. Los, *Linkages Between Global Vegetation and Climate.* PhD thesis, Vrije Universiteit and National Aeronautics and Space Administration at Goddard Space Flight Center, April 1998. Dissertation.

[3] A. P. Cracknell, *The advanced very high resolution radiometer (AVHRR).* Bristol, PA: Taylor Francis, 1997.

[4] P. J. Sellers, "Canopy reflectance, photosynthesis and transpiration," *Int. Journal of Remote Sensing*, vol. 6, pp. 1335 – 1372, 1985.

[5] J. L. Privette, C. Fowler, G. A. Wick, D. Baldwin, and W. J. Emery, "Effects of orbital drift on advanced very high resolution radiometer products: normalized difference vegetation index and sea surface temperature," *Remote sensing of enviroment*, vol. 53, pp. 164 – 171, 1995.

[6] J. Cihlar, D. Manak, and M. D'Iorio, "Evaluation of compositing algorithms for AVHRR data over land," *IEEE Transactions on Geoscience and Remote Sensing*, vol. 32, pp. 427 – 437, March 1994.

[7] S. Los, C. O. Justice, and C. J. Tucker, "A global 1^o by 1^o NDVI data set for climate studies derived from GIMMS continental NDVI data," *Int. Journal of Remote Sensing*, vol. 15, pp. 3493 – 3518, 20 November 1994.

[8] B. N. Holben, "Characteristics of maximum-value composite images from temporal AVHRR data," *Int. Journal of Remote Sensing*, vol. 7, no. 11, pp. 1417 – 1434, 1986.

[9] J. E. Pinzón, J. Pierce, C. J. Tucker, and M. Brown, "Evaluating coherence of natural images by smoothness membership in besov spaces," *IEEE Transactions on Geoscience and Remote Sensing*, vol. 39, pp. 1879 – 1889, September 2001.

[10] R. B. Myneni, I. Impens, and Asrar, "Simulation of space measurements of vegetation canopy bidirectional reflectance factors," *Remote Sensing Rev.*, vol. 7, pp. 19–41, 1993.

[11] P. J. Sellers, S. O. Los, C. J. Tucker, G. J. Collatz, C. O. Justice, D. A. Dazlich, and D. A. Randall, "A global 1^o by 1^o NDVI data set for climate studies. part 2: the generation of global fields of terrestrial biophysical parameters from the ndvi," *Int. Journal of Remote Sensing*, vol. 15, no. 17, pp. 3519 – 3545, 1994.

[12] N. Gershenfeld, *The nature of mathematical modeling.* Cambridge, U.K.: Cambridge University Press, 1999.

[13] N. E. Huang, Z. Shen, S. R. Long, M. C. Wu, H. H. Shih, Q. Zheng, N.-C. Yen, C. C. Tung, and H. H. Liu, "The empirical mode decomposition and the Hilbert spectrum for nonlinear and non-stationary time series analysis," *Proc. Royal Society London A*, vol. 454, pp. 903 – 995, 1998. Reprint.

[14] N. E. Huang, Z. Shen, and S. R. Long, "A new view of nonlinear water waves: the Hilbert spectrum," *Annu. Rev. Fluid Mech.*, vol. 31, pp. 417 – 457, 1999. Reprint.

[15] R. L. Mahoney, C. J. Tucker, A. Anyamba, M. Brown, D. Slayback, S. Los, J. Pinzon, J. Kendall, E. Pak, Z. Bronder, D. Grant, M. Paris, and A. Morahan, "Global remote sensing of vegetation from space by the NASA/GSFC GIMMS group," in *International Worshop on Global Change* (J. Kudoh and K. Yamada, eds.), Sendai Kiodo Printing Co. Ltd., 2001.

[16] R. B. Myneni, C. D. Keeling, C. J. Tucker, G. Asrar, and R. R. Nemani, "Increased plant growth in the northern high latitudes from 1981-1991," *Nature*, vol. 386, pp. 698 – 702, 1997.

[17] R. K. Kaufmann, L. Zhou, Y. Knyazikhin, N. V. Shabanov, R. B. Myneni, and C. J. Tucker, "Effect of orbital drift and sensor changes on the time series of AVHRR vegetation index data," *IEEE Transactions on Geoscience and Remote Sensing*, vol. 38, pp. 2584 – 2597, Nov. 2000.

[18] C. J. Tucker, D. Slayback, J. E. Pinzon, S. Los, R. B. Myneni, and M. G. Taylor, "Higher northern latitude normalized difference vegetation index and growing season trends from 1982 to 1999," *Int. Journal of Biometeorology*, vol. 45, pp. 184 – 190, 2001.

[19] D. A. Slayback, J. E. Pinzón, S. O. Los, and C. J. Tucker, "Northern hemisphire photosynthetic trends," *Global Change Biology*, 2002. To appear.

[20] G. G. Gutman, "On the use of long-term global data of land reflectances and vegetation indices derived from the advanced very high resolution radiometer," *Journal of Geophysical Research*, vol. 104, no. D6, pp. 6241 – 6255, 1999.

[21] S. E. Nicholson, C. J. Tucker, and M. B. Ba, "Desertification, drought, and surface vegetation: An example from the west African Sahel," *Bulletin of the American Meteorological Society*, vol. 79, pp. 815 – 829, May 1998.

[22] S. Los, G. J. Collatz, L. Bounoua, P. J. Sellers, and C. J. Tucker, "Interannual variation in global vegetation, precipitation, land-surface temperature and sea-surface temperature during the 1980s," *Journal of Climate*, p. in press, 2001.

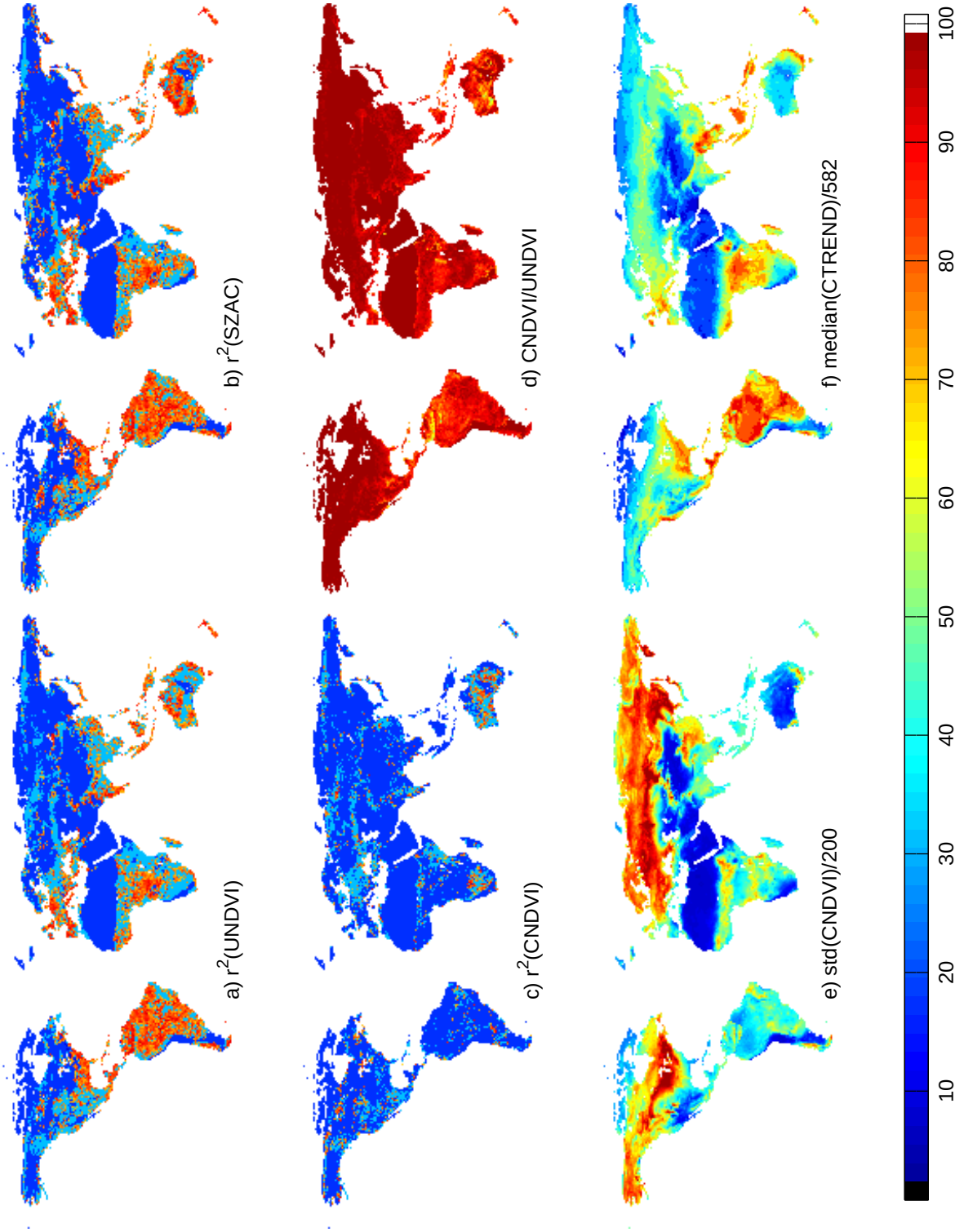

Fig. 4. Coefficient of determination between SZA trends and (a) uncorrected NDVI trend (undvi), (b) predicted SZA trend (t_{szac}), and (c) SZA-corrected NDVI trend (cndvi); (d) ratio between variances of SZA-corrected and uncorrected NDVI; (e) variance of corrected NDVI normalized by maximum variance (200); (f) temporal median value of corrected NDVI trends normalized by its maximum median value (582) with 12 levels of variation (uniform quatization).